energies

MDPI

Article

Multi-Objective Optimization of Nozzle Closing Strategies for High Head Pelton Turbines to Shorten the Nozzle Closing Time and Mitigate Water Hammer Effects

Jintao Shi [1], Chang Liu [1,*] and Lei Chen [2]

[1] State Key Laboratory of Hydroscience and Engineering, Department of Energy and Power Engineering, Tsinghua University, Beijing100084, China; shijt24@mails.tsinghua.edu.cn
[2] China Datang Corporation Science & Technology General Research Institute Hydropower Branch, Chengdu 610036, China; dtsdy_hydrop_cl@163.com
* Correspondence: liu-chang@mail.tsinghua.edu.cn

Abstract

The rapid shutdown of high-head and large-capacity Pelton turbines equipped with long penstocks often induces severe water hammer effects, threatening the structural safety of the diversion system. Traditional linear or simple piecewise nozzle closing laws struggle to achieve an optimal balance between shortening the nozzle closing time and suppressing the maximum transient pressure. To address this issue, this study proposes a multi-objective optimization framework for the non-linear nozzle-closing strategy of a large-capacity six-nozzle Pelton turbine. A one-dimensional transient flow model of the complex diversion system was established and solved using the Method of Characteristics (MOC). Subsequently, the Non-dominated Sorting Genetic Algorithm II (NSGA-II) was coupled with the model to globally optimize the discretized 10-segment nozzle-closing trajectory. The optimization objectives were to minimize both the total closing time and the maximum pressure before the nozzle. The results demonstrate that the NSGA-II algorithm autonomously converges to a "Fast-Slow-Fast" non-linear closing pattern. Compared to the baseline linear closing strategy, the optimized trajectory reduces the total shutdown time by 7.22% (from 18.15 s to 16.84 s) and decreases the maximum pressure before the nozzle by 7.61 m, effectively mitigating the net water hammer pressure rise by 13.40%. Physical mechanism analysis reveals that the intermediate "slow" phase effectively staggers the constructive superposition of reflected positive water hammer waves, achieving an active peak-shifting effect. This study can provide a theoretical reference for the safe and efficient shutdown control of large-capacity Pelton turbines.

Keywords: Pelton turbine; water hammer effect; multi-objective optimization; nozzle-closing strategy

Check for updates

Received: 22 May 2026
Revised: 23 June 2026
Accepted: 2 July 2026
Published: 3 August 2026

Copyright: © 2026 by the authors. Licensee MDPI, Basel, Switzerland. This article is an open access article distributed under the terms and conditions of the Creative Commons Attribution (CC BY) license.

1. Introduction

Under the guidance of addressing global climate change and achieving the "dual carbon goals," the penetration of intermittent renewable energy sources, particularly wind and photovoltaic power, has continued to increase [1]. Because their output is inherently variable, modern power systems require stronger capabilities in frequency regulation, peak shaving, and fast reserve deployment. Hydropower units, characterized by rapid start-up and shutdown response capabilities, wide operating range, and high controllability, have therefore become an essential flexible resource for maintaining grid stability.

As hydropower development increasingly shifts to high-altitude regions with large available heads, Pelton turbines have been widely adopted due to their suitability for high-head operation and their broad high-efficiency range. For example, 500 MW six-nozzle Pelton units are being deployed at the Zala Hydropower Station in Xizang, China [2]. Such high-capacity Pelton units are commonly equipped with ultra-long penstocks and operate under extremely high heads, which makes the hydraulic transient problem during shutdown particularly critical. When the nozzle closes rapidly, the flow velocity in the penstock changes abruptly, generating severe water hammer. Excessive transient pressure may endanger the structural integrity of the penstock and its associated components and, in extreme cases, may even lead to catastrophic failures [3]. Conversely, slowing down the nozzle closure to mitigate pressure rise may prolong the shutdown process and compromise operational efficiency and emergency response capability. Consequently, a key control challenge for high-head Pelton hydropower plants is to achieve a better compromise between two competing objectives: shortening the nozzle-closing time and suppressing the maximum transient pressure.

In terms of numerical modeling, the one-dimensional transient-flow equations solved by the Method of Characteristics (MOC) have long been established as a reliable and extensively validated framework for simulating hydraulic transients in pressurized conduits. Pal et al. [4] systematically reviewed the principal numerical approaches to water-hammer modeling and concluded that the MOC remains the most widely adopted method, owing to its accuracy, computational efficiency, and intuitive treatment of boundary conditions. The reliability of the MOC has been repeatedly confirmed against analytical solutions, benchmark problems, and experimental data: Wang et al. [5] verified MOC-based predictions of water hammer in uniform- and variable-area ducts and in surge-tank systems against analytical and CFD results, while Nicolet et al. [6] employed an equivalent one-dimensional model of galleries and penstocks derived from the same hyperbolic equations to reproduce the field-measured transient behavior of a hydropower plant. Adamkowski et al. [7] further provided experimental verification of 1D water-hammer simulations. These studies collectively demonstrate that the 1D MOC framework adopted herein is a mature and trustworthy tool for transient-pressure prediction in long-penstock systems such as the one considered in this study. Regarding the governing equations, the complete forms retain the convective-acceleration terms; however, in typical water-hammer problems, the pressure-wave speed greatly exceeds the flow velocity, so that the temporal variations in head and discharge dominate over their spatial convective counterparts. As summarized by Pal et al. [4], the nonlinear convective terms are comparatively small and can be justifiably neglected, and this simplification has been widely adopted in subsequent transient modeling of penstock–turbine systems.

A substantial body of research has investigated shutdown and transient control strategies for hydropower units. Conventional approaches typically employ linear or simple two-stage piecewise closing laws [8]. With advances in hydraulic transient theory and engineering practice, it has been recognized that non-linear closing schemes such as three-stage or delayed-closing patterns can provide improved pressure mitigation potential [9,10]. Recent theoretical analyses of slow valve maneuvers have further elucidated the complex non-linear coupling between hydraulic head and flow velocity during transients [11]. Furthermore, experimental and numerical studies on long-distance pipelines and micro-hydroelectric systems have demonstrated that optimized multi-stage (e.g., fast-slow) or combined valve-closing strategies can significantly reduce the maximum water hammer pressure compared to traditional linear closures [12,13]. Lai et al. [14] proposed a three-stage guide-vane strategy (“close–open–close”) for reaction turbines, and related studies examined coordinated closing laws between guide vanes and inlet valves. In

parallel, optimization methodologies have evolved from experience-based trial-and-error tuning to intelligent algorithms [15]. In recent years, multi-objective optimizers such as the Non-dominated Sorting Genetic Algorithm II (NSGA-II) and multi-objective particle swarm optimization (MOPSO) have been used to calibrate control parameters in hydraulic transients [16], providing Pareto-optimal solutions that balance rotational speed and pressure constraints. Moreover, novel heuristic algorithms, such as the multi-objective coati optimization algorithm, have been successfully applied to the joint optimal operation of pumps and valves in complex long-distance water conveyance systems, proving the superiority of intelligent algorithms in handling multi-variable transient control problems [17].

Nevertheless, most existing studies focus on guide-vane control of Francis turbines and pump-turbines [18,19], whereas the governing mechanism for multi-nozzle Pelton turbines differs considerably. For Pelton units, flow regulation is achieved by needle motion in multiple nozzles that jointly generate free jets intercepted by the runner, rather than by guide-vane modulation of internal flow passages [20]. Moreover, for diversion systems extending hundreds of meters or more, pressure-wave propagation, reflection, and superposition become highly intricate. Under such conditions, linear or coarse piecewise closing laws often fail to effectively de-phase reflected pressure peaks, making it difficult to reduce the nozzle-closing time while also limiting the peak pressure rise. These gaps motivate a refined design of non-linear nozzle-closing laws that is grounded in the physical mechanism of wave superposition and supported by advanced multi-objective optimization.

Accordingly, this study investigates a high-head Pelton hydropower station in China by employing a one-dimensional transient flow equation and employing the Method of Characteristics (MOC) for explicit finite difference solution, calculates the water hammer pressure variation pattern under the initial strategy of linear nozzle closure, and solves and compares the two-stage and three-stage closure patterns. Ultimately, a nozzle closure strategy for Pelton turbines based on the NSGA-II algorithm is proposed, achieving a comprehensive enhancement in both reducing the nozzle-closing time and lowering the maximum pressure upstream of the nozzle.

2. Methodology

2.1. Pipeline and Turbine Model

Pelton turbines are typically subjected to extremely high heads and equipped with long water diversion penstocks (e.g., the Zala Hydropower Station's pipe exceeds 5000 m). Closing the nozzles too quickly can cause a sharp pressure surge, inducing severe water hammer effects. The water flow in the penstock exhibits obvious one-dimensional transient flow characteristics. The continuity and momentum equations for the one-dimensional transient flow elastic water hammer model [21] are expressed as follows:

$$\frac{\partial H}{\partial t} - \frac{a^2}{gA}\frac{\partial Q}{\partial x} + \frac{Q}{A}\sin\theta - \frac{Q}{A}\frac{\partial H}{\partial x} = 0 \tag{1}$$

$$\frac{\partial Q}{\partial t} - gA\frac{\partial H}{\partial x} + \frac{\lambda Q|Q|}{2DA} + \frac{Q\partial Q}{gA\partial x} = 0 \tag{2}$$

where H is the piezometric head, Q is the discharge, a is the water hammer pressure wave velocity, x is the spatial coordinate calculated from the downstream valve upwards, A is the cross-sectional area of the pipe, θ is the pipe inclination angle, D is the pipe diameter, λ is the friction loss coefficient, and g is the gravitational acceleration.

Since the variations in discharge and head along the pipeline are much smaller than their variations over time (i.e., $\frac{\partial Q}{\partial x} \ll \frac{\partial Q}{\partial t}$ and $\frac{\partial H}{\partial x} \ll \frac{\partial H}{\partial t}$), the convective acceleration terms can be neglected [4]. The governing equations are thus simplified to:

$$\frac{\partial H}{\partial t} - \frac{a^2}{gA}\frac{\partial Q}{\partial x} + \frac{Q}{A}\sin\theta = 0 \tag{3}$$

$$\frac{\partial Q}{\partial t} - gA\frac{\partial H}{\partial x} + \frac{\lambda Q|Q|}{2DA} = 0 \tag{4}$$

The Pelton turbine acts as the downstream boundary condition for the pipeline model. Its dynamic behavior during shutdown involves the nozzle flow characteristics and the rotor's mechanical rotation. Before the generator is disconnected from the grid, the rotational speed is maintained at the rated synchronous speed ($\omega = \omega_r$). Once the nozzle opening drops below the no-load opening threshold, the unit is disconnected from the grid, and the rotational speed is governed by the rigid rotor mechanical equation:

$$J\frac{d\omega}{dt} = T_{jet} - T_0 \tag{5}$$

where J is the moment of inertia of the entire rotating mass (including the turbine and generator rotors), and T_0 is the resistance torque. This dynamic equation is integrated over time to predict the maximum rotational speed during the final stage of the shutdown process. The hydraulic torque T_{jet} generated by the jet is calculated based on the momentum theorem:

$$T_{jet} = \sum_{i=1}^{Z} F_{Ui}\frac{D_1}{2} \tag{6}$$

where F_{Ui} is the tangential force generated by the i-th nozzle, Z is the number of operating nozzles, and D_1 is the pitch circle diameter of the runner. Based on the momentum theorem and Newton's third law, tangential force for the i-th nozzle is expressed [22] as:

$$F_{Ui} = \rho_l Q_i\left[V_j cos(\theta) - U_1\right]\left[1 - cos(\beta_2)\right] \tag{7}$$

where ρ_l is the water density, Q_i is the discharge of the i-th nozzle, β_2 is the relative exit angle of the jet, and θ is the angular difference between the bucket's current position and the perpendicular impact position. The discharge Q_i of each nozzle is determined by its relative needle stroke Y_i. The flow coefficient, defined as the ratio of the actual discharge to the theoretical discharge based on the nozzle diameter, can be fitted as a fourth-order polynomial based on experimental data:

$$\varphi_i = f(Y_i) \tag{8}$$

Consequently, the discharge Q_i for each nozzle is expressed as:

$$Q_i = \varphi_i\frac{\pi D_0^2}{4}V_j \tag{9}$$

The jet velocity V_j and the peripheral velocity of the runner U_1 are given by:

$$V_j = \sqrt{\xi \cdot 2gH} \tag{10}$$

$$U_1 = \frac{\omega D_1}{2} \tag{11}$$

where ξ is the nozzle energy loss coefficient, and H is the operating head, which couples with the pipeline transient model.

2.2. Method of Characteristics and Discrete Solution

To solve the simplified partial differential equations, the MOC is employed [23]. This method transforms the partial differential equations into compatibility equations along specific characteristic lines.

Along the positive characteristic line C^+ ($\frac{dx}{dt} = a$), meaning the pressure wave propagates from upstream to downstream at velocity a, the compatibility equation is written as:

$$\frac{dH}{dt} + \frac{a}{gA}\frac{dQ}{dt} + \frac{a\lambda}{2gDA^2}Q|Q| - \frac{Q}{A}sin\theta = 0 \tag{12}$$

Along the negative characteristic line C^- ($\frac{dx}{dt} = -a$), meaning the pressure wave reflects from downstream to upstream at velocity a, the compatibility equation is written as:

$$\frac{dH}{dt} - \frac{a}{gA}\frac{dQ}{dt} - \frac{a\lambda}{2gDA^2}Q|Q| - \frac{Q}{A}sin\theta = 0 \tag{13}$$

To facilitate the numerical solution, the equations are discretized using a first-order finite difference scheme. The pipeline is divided along its axis into N equal segments with a spatial step $\Delta x = L/N$. According to the Courant stability condition, the time step is selected as $\Delta t = \Delta x/a$ [7]. By integrating the differential equations along the characteristic lines, the algebraic compatibility equations for calculating the head and discharge at the i-th node at time t are obtained.

The algebraic equation along the positive characteristic line C^+ is:

$$H_i + \frac{a}{gA}Q_i = H_{i-1} + \frac{a}{gA}Q_{i-1} - \frac{\lambda\Delta x}{2gDA^2}Q_{i-1}|Q_{i-1}| + \frac{Q_{i-1}}{A}sin\theta_{i-1}\Delta t \tag{14}$$

The algebraic equation along the negative characteristic line C^- is:

$$H_i - \frac{a}{gA}Q_i = H_{i+1} - \frac{a}{gA}Q_{i+1} + \frac{\lambda\Delta x}{2gDA^2}Q_{i+1}|Q_{i+1}| - \frac{Q_{i+1}}{A}sin\theta_{i+1}\Delta t \tag{15}$$

To simplify the expressions, known variables from the previous time step are grouped into constants C_{i-1}, C_{i+1} and the pipeline characteristic impedance B:

$$C_{i-1} = H_{i-1} + \frac{a}{gA}Q_{i-1} - \frac{\lambda\Delta x}{2gDA^2}Q_{i-1}|Q_{i-1}| + \frac{Q_{i-1}}{A}sin\theta_{i-1}\Delta t \tag{16}$$

$$C_{i+1} = H_{i+1} - \frac{a}{gA}Q_{i+1} + \frac{\lambda\Delta x}{2gDA^2}Q_{i+1}|Q_{i+1}| - \frac{Q_{i+1}}{A}sin\theta_{i+1}\Delta t \tag{17}$$

$$B = \frac{a}{gA} \tag{18}$$

By solving the system of equations simultaneously, the explicit formulas for the head H_i and discharge Q_i at internal nodes for the current time step are derived.

$$H_i = \frac{C_{i-1} + C_{i+1}}{2} \tag{19}$$

$$Q_i = \frac{C_{i-1} - C_{i+1}}{2B} \tag{20}$$

To complete the flow solution, appropriate boundary conditions must be applied at the ends of the pipeline system [24]. At the upstream boundary (node 0), the water level is assumed to be constant, represented by the upstream reservoir head H_0. Substituting H_0

into the algebraic equation of the negative characteristic line, the discharge at the upstream boundary is calculated as:

$$Q_0 = \frac{H_0 - C_{i+1}}{B} \tag{21}$$

At the downstream boundary (node $N + 1$), the discharge Q_{N+1} is governed by the dynamic opening of the Pelton turbine nozzles. The relationship between the nozzle stroke and the flow coefficient is determined by the turbine's dynamic model. Substituting this relationship into the algebraic equation of the positive characteristic line, the water hammer pressure in front of the downstream nozzle is obtained:

$$H_{N+1} = C_{i-1} - BQ_{N+1} \tag{22}$$

By coupling these boundary conditions with the internal node equations, the transient pressure and discharge variations throughout the entire pipe during the nozzle-closing process can be accurately simulated step by step.

3. Multi-Objective Optimization Model and Solution Method

3.1. Optimization Objectives

The core of optimizing the normal shutdown of a Pelton turbine lies in resolving two conflicting engineering requirements. On the one hand, to disconnect the unit safely and quickly while reducing idling wear, the nozzle-closing time should be minimized. On the other hand, to ensure the structural safety of the long penstock and the turbine, the sudden increase in water hammer pressure caused by rapid nozzle closure must be strictly controlled. Thus, the model sets the following two optimization objectives:

(1) Minimize total nozzle-closing time

The time required for the nozzles to fully close from their initial opening to zero is defined as the total nozzle-closing time T_{total}. The objective function f_1 is expressed as:

$$f_1 = minT_{total} = min\sum_{i=1}^{n} \Delta t_i \tag{23}$$

where n is the number of control segments into which the nozzle-closing process is divided, and Δt_i is the time consumed during the i-th closing segment.

(2) Minimize maximum water hammer pressure in front of the needle

Throughout the dynamic shutdown process, the transient pressure in front of the needle (i.e., at the terminal node $N + 1$ of the pipeline) fluctuates violently due to the propagation and superposition of water hammer waves [25]. The objective function f_2 aims to minimize the peak pressure during this process:

$$f_2 = minH_{max} = min\left(max_{t\in[0,T_{total}]} H_{N+1}(t)\right) \tag{24}$$

where $H_{N+1}(t)$ is the dynamic head in front of the needle at time t, obtained by solving the coupled MOC and turbine dynamic model.

Since the algorithm yields a set of the Pareto front solutions rather than a single optimal solution, a systematic multi-attribute decision-making methodology is required to select the final compromise strategy. In this study, Min-Max normalization combined with a Simple Additive Weighting (SAW) method is employed. First, to eliminate the dimensional

differences between the total closing time (seconds) and the maximum pressure (meters), the objective values of the Pareto solutions are normalized into a dimensionless range of [0, 1]:

$$\overline{f_{1,i}} = \frac{f_{1,i} - f_{1,min}}{f_{1,max} - f_{1,min}} \tag{25}$$

$$\overline{f_{2,i}} = \frac{f_{2,i} - f_{2,min}}{f_{2,max} - f_{2,min}} \tag{26}$$

where $f_{1,i}$ and $f_{2,i}$ are the total closing time and maximum pressure of the i-th Pareto solution, respectively. The subscripts min and max denote the minimum and maximum values within the valid Pareto set. Subsequently, a composite score for each solution is calculated:

$$f = \omega_1 \overline{f_{1,i}} + \omega_2 \overline{f_{2,i}} \tag{27}$$

where ω_1 and ω_2 are the weighting factors for the two objectives. In this study, equal weights ($\omega_1 = \omega_2 = 0.5$) are assigned, reflecting an engineering preference that considers the rapid disconnection of the unit and the structural safety of the penstock to be of equal importance.

3.2. Decision Variables

To enable the optimization algorithm to flexibly search for various non-linear closing laws, this study adopts an equal-opening segmentation method to parameterize the needle closing curve. The total opening to be closed (from the initial double-nozzle opening to fully closed) is evenly divided into n equal intervals, meaning each segment covers $1/n$ of the total closing stroke. The time duration Δt_i experienced for each segment's opening change is taken as the decision variable. Therefore, the decision variable X can be expressed as:

$$X = \{\Delta t_1, \Delta t_2, \cdots, \Delta t_n\} \tag{28}$$

By varying the magnitude of each component in vector X, the closing rate of the nozzles at different stages can be precisely controlled, thereby generating any monotonically decreasing non-linear closing curve.

3.3. Constraints

To ensure that the optimized shutdown strategy is executable in practical engineering and strictly superior to traditional strategies, the model must satisfy the following constraints:

(1) Nozzle opening rate constraint

Limited by the physical performance of the servomotor and hydraulic control system, the closing rate of the nozzles cannot be infinitely large. In any control segment, the closing rate must be less than or equal to the maximum allowable closing rate R_{max}.

$$\left| \frac{dY_i}{dt} \right| \leq R_{max} \tag{29}$$

(2) Decision variable bounds constraint

To prevent a single segment's closing time from being too short (causing local rate violations) or too long (deteriorating the overall nozzle-closing time), reasonable search spaces are set for the segment duration Δt_i based on engineering experience:

$$\Delta t_{min} \leq \Delta t_i \leq \Delta t_{max} (i = 1, 2, \cdots, n) \tag{30}$$

(3) Dynamic Boundary Condition

During the nozzle-closing process of a Pelton turbine, the rotational speed of the turbine exhibits distinct dynamic characteristics depending on its operational stage [26]. To ensure the physical accuracy of the transient simulation, the model strictly constrains the rotational speed $\omega(t)$ based on the grid connection status and the no-load opening threshold: in the initial phase of nozzle closure, when the total nozzle opening is greater than the no-load opening, the unit is assumed to remain synchronized with the power grid. During this period, the rotational speed is rigidly constrained to the rated speed ω_r.

Once the nozzle opening drops to or below the no-load opening, the unit disconnects from the grid. The rotational speed is no longer constant but is governed by the rotor dynamics equation, which is determined by the unbalanced torque (the difference between the hydrodynamic driving torque and the constant resistance torque) and the rotational inertia J.

3.4. Model Solution Based on NSGA-II

To solve the formulated multi-objective optimization model, the Non-dominated Sorting Genetic Algorithm II (NSGA-II) is employed. The problem is a two-objective, continuous, and relatively low-dimensional optimization in which the evaluation of every candidate solution requires a complete MOC transient simulation, making function evaluations computationally expensive. NSGA-II is particularly well suited: its fast non-dominated sorting mechanism and crowding-distance assignment ensure both convergence toward the Pareto-optimal front and a uniform diversity of solutions [27], while its elitist, parameter-light structure attains a well-resolved front within a limited number of evaluations, without the problem-specific reference-vector or swarm-parameter tuning required by decomposition swarm-based alternatives. By coupling the NSGA-II algorithm with the transient flow Method of Characteristics model, we globally optimize the n-segment nozzle-closing trajectory to minimize both the total nozzle-closing time and the maximum transient pressure, while strictly satisfying the physical constraints such as the maximum nozzle-closing rate. The specific solution process of this optimization framework is illustrated in Figure 1.

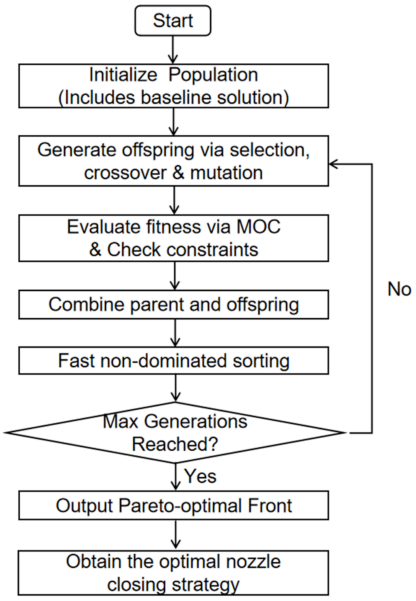


Figure 1. Flowchart of the multi-objective optimization framework coupling the NSGA-II algorithm with the MOC transient flow solution.

4. Case Study

4.1. Engineering Background and Parameters

To verify the multi-objective optimization model, the Zala Hydropower Station in Xizang, China, was selected as the engineering case. The station is equipped with 510 MW six-nozzle Pelton turbines, which are currently the largest-capacity Pelton turbines in the world. The diversion system has a total equivalent pipe length exceeding 5500 m.

The normal nozzle-closing process analyzed in this study begins when the turbine load drops and the operating nozzles are reduced to two symmetrical nozzles, with an initial relative stroke of 0.605 each, making the total initial opening 1.21. The process ends when the nozzles are fully closed. When the total opening drops below the no-load opening threshold, the generator is disconnected from the grid, and the rotational speed begins to fluctuate based on the unbalanced torque. The key parameters of the turbine and the diversion system are listed in Table 1.

Table 1. Key parameters of the Pelton turbine.

Parameter	Symbol	Value	Unit
Rated head	H_{rated}	671	m
Rated rotation speed	n_{rated}	214.3	rpm
Runner pitch circle diameter	D_1	4.95	m
Nozzle diameter	D_0	0.522	m
Moment of inertia	J	11,525,000	kg·m^2

The diversion system is highly complex, consisting of multiple intakes, diversion tunnels, and penstocks with varying diameters and inclination angles. The upstream reservoir water level is 2815.00 m, and the nozzle installation elevation is 2127.60 m, providing an initial static head of 687.40 m. The water hammer wave velocity a is taken as 1000 m/s. The overall layout of the water conveyance system, including the upstream reservoir, intake, diversion tunnel, pressure penstock, and the distributor ring connected to the Pelton turbine, is schematically illustrated in Figure 2. As shown in Figure 2, the diversion tunnel is discretized into 12 segments and the pressure penstock into 11 segments along the flow direction, with Node 0 located at the upstream reservoir boundary condition for the MOC solution.

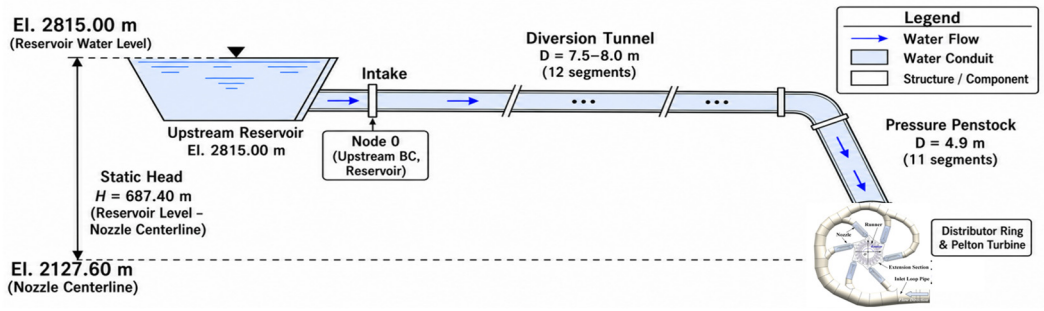


Figure 2. Schematic layout of the diversion system of the case study hydropower station.

On this basis, the detailed geometric and hydraulic parameters of the diversion pipeline system are partially listed in Table 2.

4.2. Transient Characteristics of the Initial Linear Closing Strategy

In conventional engineering practice, the nozzles of a Pelton turbine are typically closed at a constant linear rate during a normal shutdown. To establish a baseline for comparison, an initial linear closing strategy was simulated, where the relative stroke of

each nozzle decreases at a constant rate of 1/30 per second (i.e., it would take 30 s for a nozzle to close from a fully open state of 1.0 to 0). Given the initial relative stroke of 0.605, this results in a total closing time of 18.15 s.

Table 2. Parameters of the diversion pipeline system (Partial).

No.	Component	Diameter (m)	Length (m)	Loss Coefficient	Start Elevation (m)	End Elevation (m)
1	Intake 1	9.010	4.40	2.87×10^{-6}	2800.75	2800.75
2	Intake 2	8.463	3.30	1.73×10^{-6}	2800.75	2800.75
3	Diversion tunnel 1	7.996	12.00	6.14×10^{-7}	2800.75	2800.75
...	Diversion tunnel 2~11	...	3744.68	...	2800.75	2761.10
14	Diversion tunnel 12	7.500	10.85	1.24×10^{-6}	2761.10	2761.10
15	Unit 1 penstock 1	4.900	76.90	4.28×10^{-7}	2761.10	2759.80
...	Unit 1 penstock 2~10	...	1631.21	...	2759.80	2127.60
25	Unit 1 penstock 11	2.900	39.27	6.97×10^{-6}	2127.60	2127.60
26	Distributor ring	2.900	70.00	3.52×10^{-8}	2127.60	2127.60

To ensure the accuracy and reliability of the numerical simulation while balancing computational efficiency, a spatial step independence test was conducted before the formal transient calculations. Using the initial linear closing strategy as the test case, various spatial steps (Δx) and their corresponding time steps ($\Delta t = \Delta x/a$) were evaluated. The maximum water hammer pressures in front of the needle under different discretizations are compared in Table 3.

Table 3. Maximum pressure in front of the needle under different spatial and time steps.

Spatial Step (m)	Time Step (s)	Maximum Pressure (mH_2O)
1111	1.11	744.09
278	0.278	744.16
92.6	0.093	744.17
27.8	0.028	744.17
11.1	0.011	744.17

As shown in Table 3, the calculated maximum pressure converges and stabilizes at 744.17 m when the spatial step is reduced to 92.6 m. Further refinement of the grid yields no significant change in the results but substantially increases the computational load. Therefore, a spatial step of Δx = 92.6 m and a time step of Δt = 0.093 s were selected for all subsequent MOC simulations in this study. The transient flow calculation results for the initial linear closing strategy, using the selected steps, are illustrated in Figure 3.

As shown in Figure 3, under this linear closing law, the total nozzle-closing time is 18.15 s. The maximum water hammer pressure in front of the needle reaches 744.17 m, and the maximum rotational speed of the unit slightly rises to 214.35 rpm. While this baseline strategy satisfies the basic safety requirements for the transition process, the pressure surge is still significant, indicating that there is considerable room for optimization in terms of shortening the nozzle-closing time and suppressing the water hammer pressure.

4.3. Comparison of Typical Piecewise Closing Strategies

To explore the influence of non-linear nozzle-closing laws on the maximum transient pressure, various "two-stage" and "three-stage" closing strategies were evaluated. To ensure a fair comparison, the total closing time was kept identical to the initial linear strategy (18.15 s).

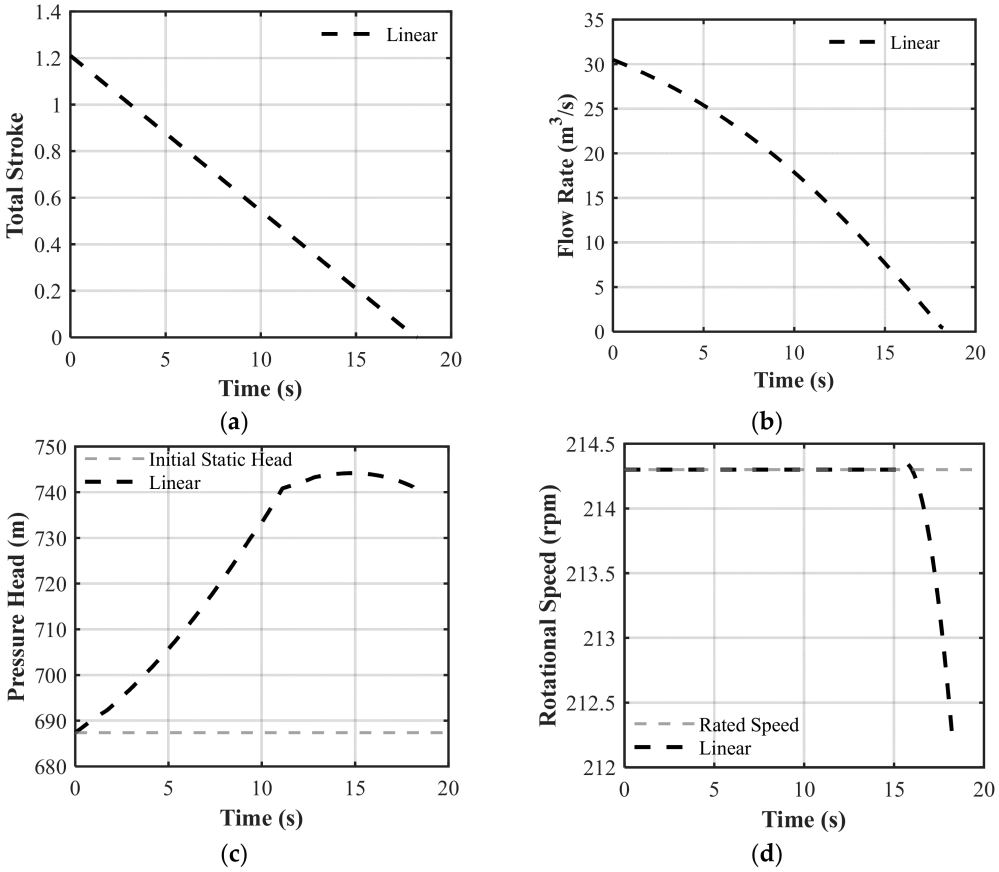


Figure 3. Transient performance of the initial linear closing strategy: (**a**) total nozzle opening; (**b**) total discharge; (**c**) pressure in front of the needle; (**d**) rotational speed.

First, two typical two-stage laws were simulated: a "fast-slow" strategy, which closes 60% of the opening in the first 40% of the time and the remaining 40% in the last 60% of the time; and a "slow-fast" strategy, which closes 40% of the opening in the first 60% of the time and the remaining 60% in the last 40% of the time. Calculation results are illustrated in Figure 4.

As shown in Figure 4, both two-stage strategies performed worse than the linear strategy in suppressing the water hammer effect. The maximum pressures for the fast-slow and slow-fast strategies reached 758.43 m and 764.12 m, respectively.

Subsequently, two three-stage laws were evaluated to further investigate the pressure response. The "fast-slow-fast" strategy closes 40% of the opening in the first 30% of the time, 20% in the middle 40% of the time, and the remaining 40% in the final 30% of the time. Conversely, the "slow-fast-slow" strategy closes 30% of the opening in the first 35% of the time, 40% in the middle 30% of the time, and the remaining 30% in the final 35% of the time. The transient simulation results are illustrated in Figure 5.

As shown in Figure 5, the fast-slow-fast strategy is significantly superior. It successfully reduced the maximum pressure to 733.93 m, achieving a 10.24 m reduction compared to the baseline linear strategy. In contrast, the slow-fast-slow strategy yielded a higher peak pressure of 752.64 m. These comparisons reveal that the closing rate distribution at different stages critically impacts the maximum water hammer pressure, highlighting the strong potential of "fast-slow-fast" patterns for further optimization.

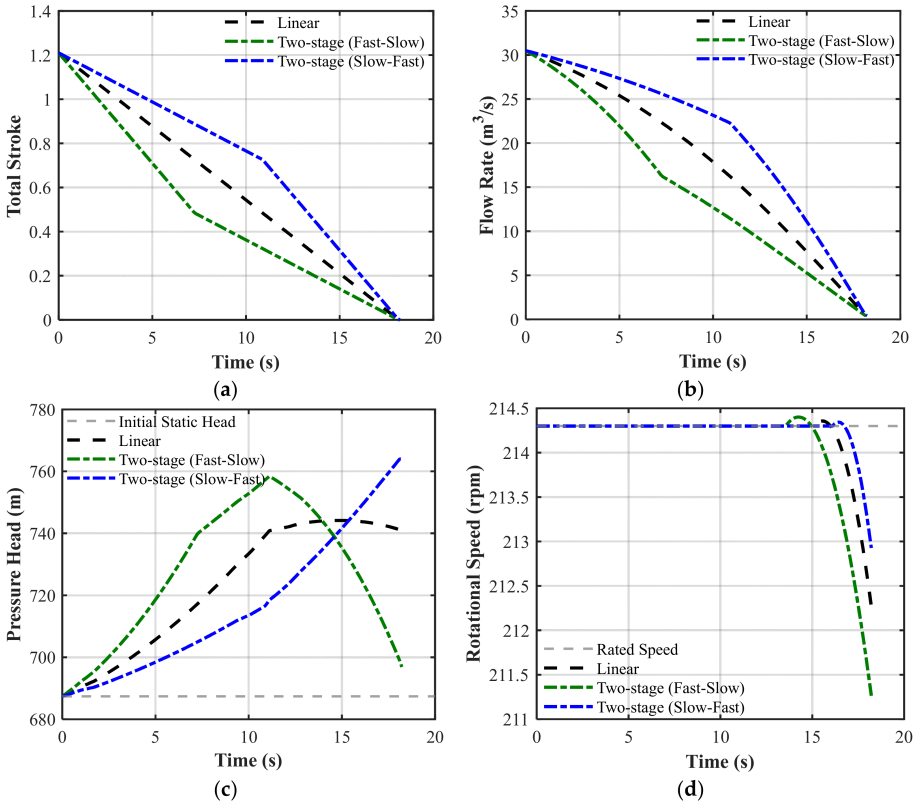


Figure 4. Comparison between two-stage closing strategies and the initial linear strategy: (**a**) total nozzle opening; (**b**) total discharge; (**c**) pressure in front of the needle; (**d**) rotational speed.

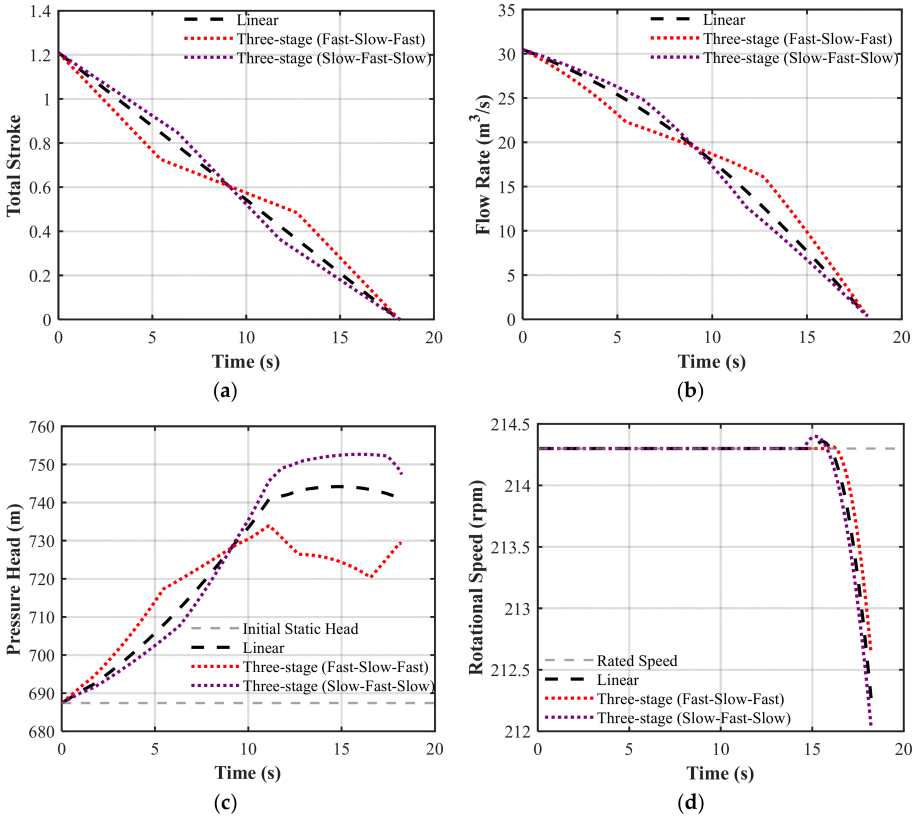


Figure 5. Comparison between three-stage closing strategies and the initial linear strategy: (**a**) total nozzle opening; (**b**) total discharge; (**c**) pressure in front of the needle; (**d**) rotational speed.

4.4. Multi-Objective Optimization Results Based on NSGA-II

To simultaneously minimize the total shutdown time and the maximum transient pressure, the NSGA-II algorithm was applied to globally optimize the closing trajectory. The nozzle-closing stroke was discretized into n equal segments (each representing $1/n$ of the total opening to be closed). Since the selected segment number (n) directly affects the dimensionality of the solution space, the quality of the Pareto front, and the computational effort, a sensitivity study was conducted to justify the choice of n. Five different segment numbers (n = 5, 10, 15, 20, 30) were evaluated. To ensure a fair comparison across different dimensions, several adaptive constraints were implemented in the NSGA-II algorithm:

(1) Population Size Scaling: The population size was dynamically scaled with the segment number to maintain sufficient search density in higher-dimensional spaces.
(2) Adaptive Time Bounds: The search bounds for the duration of each segment were inversely scaled with n, ensuring that the overall time constraints remained consistent and fair across all cases.
(3) Convergence-Based Stopping Criterion: Instead of using a fixed number of generations, the algorithm was set to stop when the Pareto front remained stable for 500 consecutive generations with a function tolerance of 10^{-5}, ensuring that each case fully converged.

The time durations of each segment served as the decision variables. The Pareto fronts for different segment numbers are compared in Figure 6, and the computational effort is summarized in Table 4.

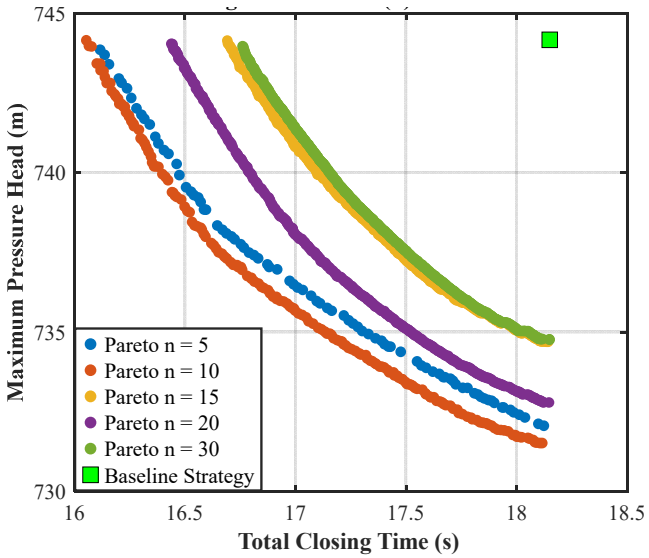


Figure 6. Pareto front for different segment numbers of the multi-objective optimization based on NSGA-II.

Table 4. Computational effort of the optimization under different segment numbers.

Number of Segments	Population Size	Relative Computational Time
5	250	1.00
10	500	2.38
15	750	3.09
20	1000	5.31
30	1500	7.41

As shown in Figure 6, the Pareto front for n = 10 is located closest to the bottom-left corner, indicating the best overall trade-off between total closing time and maximum

pressure. When n is small (n = 5), the limited control flexibility results in a slightly inferior Pareto front. Conversely, when n increases to 15, 20, or 30, despite the proportionally increased population size, the optimization suffers from the curse of dimensionality. The highly complex solution space prevents the algorithm from finding better fronts, causing the Pareto curves to shift to the top-right, indicating degraded performance. Furthermore, as shown in Table 4, the relative computational time increases significantly for larger n. Therefore, n = 10 provides the optimal balance between optimization quality and computational efficiency, justifying its selection for the subsequent decision-making process. The optimization yielded a set of non-dominated solutions forming a Pareto front, which clearly illustrates the inherent trade-off between minimizing the nozzle-closing time and suppressing the maximum water hammer pressure, as shown in Figure 7.

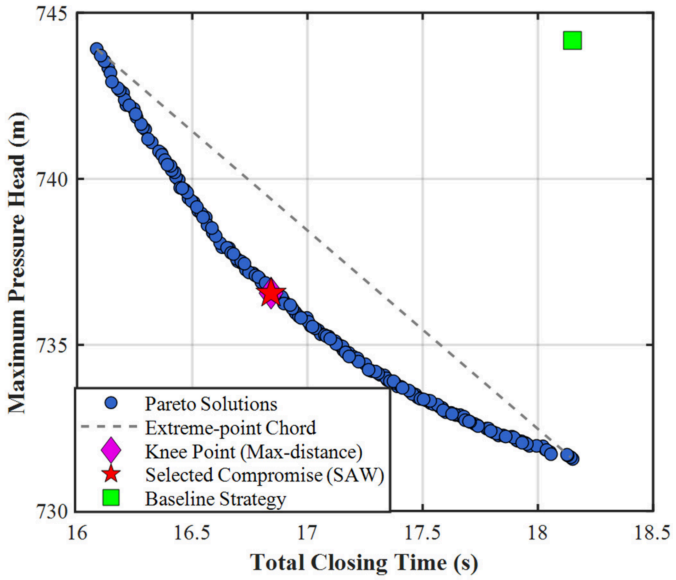


Figure 7. Pareto front of the multi-objective optimization based on NSGA-II (segment = 10).

Based on the decision-making methodology defined in Section 3.1, the final compromise solution was selected from the Pareto set. First, a filtering process was applied to retain only the solutions that strictly outperformed the baseline linear strategy (i.e., $H_{max} \leq 744.17$ m and $T_{total} \leq 18.15$ s). The selection was then carried out using two independent criteria. On the one hand, the equal-weighted SAW scoring method (Equations (25)–(27)) identified the solution with the optimal composite score at T = 16.84 s and H_{max} = 736.56 m. On the other hand, the maximum-chord-distance method located the geometric knee point—the point of maximum curvature of the front—at exactly the same solution. The fact that two methodologically independent criteria converge on an identical solution confirms that the selected strategy is an intrinsic feature of the trade-off front rather than an artifact of the assigned weights, thereby ensuring an objective and robust decision.

To further characterize the local behavior around this selected solution, the marginal rate of substitution $|dH/dT|$ between the two objectives was evaluated on both sides of the point via local linear fitting. On the left branch—corresponding to a further shortening of the closing time—the slope is $|dH/dT| = 8.33$, indicating that each additional second saved would incur a maximum-pressure rise of about 8.33 m. On the right branch—corresponding to a further reduction in pressure—the slope flattens to $|dH/dT| = 4.49$, indicating that each additional second spent would yield only about 4.49 m of pressure mitigation. The resulting 1.85-fold slope ratio reflects a clear "steep-left/flat-right" transition: moving leftward from the selected point would make time reduction disproportionately expensive

in terms of pressure, whereas moving rightward would prolong the shutdown for only a marginal pressure benefit. The optimized decision variables for this selected strategy are listed in Table 5.

Table 5. Optimized closing parameters obtained by NSGA-II.

Segment	Total Opening	Time Duration (s)	Total Time (s)
0	1.210	0	0
1	1.089	1.308	1.308
2	0.968	1.282	2.589
3	0.847	1.372	3.961
4	0.726	1.549	5.510
5	0.605	3.514	9.024
6	0.484	2.545	11.569
7	0.363	1.403	12.972
8	0.242	1.300	14.287
9	0.121	1.293	15.562
10	0	1.280	16.842

The transient performance of the optimized strategy is compared with the initial linear strategy in Figure 8, demonstrating a remarkable comprehensive improvement. Specifically, the total nozzle-closing time was reduced to 16.84 s, which is 1.31 s (7.22%) shorter than the initial linear strategy. Simultaneously, the maximum pressure in front of the needle was reduced to 736.56 m, achieving a 7.61 m decrease compared to the baseline. Considering the initial static head of 687.40 m, the optimized strategy successfully mitigated the net water hammer pressure rise by 13.40%. Furthermore, as shown in Figure 8d, the rotational speed rise is also maintained within a safe and acceptable range during the optimized shutdown process.

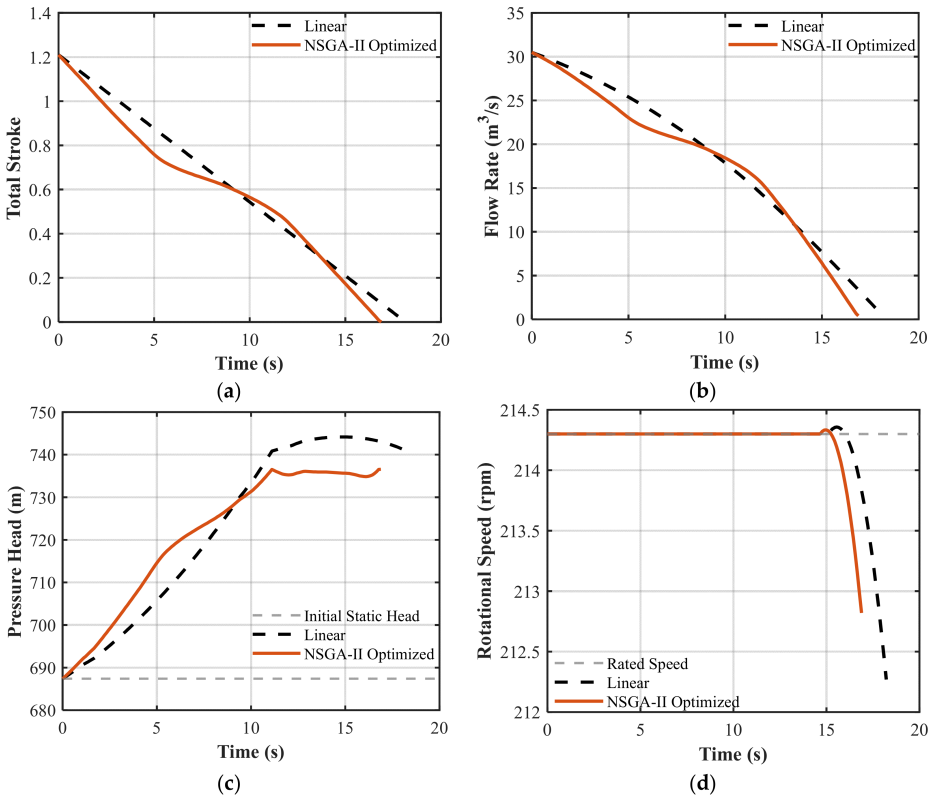


Figure 8. Comparison between the NSGA-II optimized strategy and the initial linear strategy: (**a**) total nozzle opening; (**b**) total discharge; (**c**) pressure in front of the needle; (**d**) rotational speed.

An analysis of the physical mechanism behind the optimized trajectory reveals that the NSGA-II algorithm autonomously converged to a refined "fast-slow-fast" pattern, which aligns perfectly with the principles of water hammer wave propagation and superposition in long penstocks. During the initial phase, which accounts for the first 32.7% of the total time, the nozzle closes rapidly to cover 40% of the stroke. At this stage, the generated positive water hammer wave propagates upstream, and the reflected waves have not yet returned to the nozzle, allowing the fast closing to effectively reduce the overall time without causing complex wave superposition. Subsequently, in the middle phase spanning 36.0% of the time, the nozzle closes only 20% of the stroke. This is the critical period when the first reflected positive waves return from the complex upstream pipe network. The algorithm sharply lowers the closing rate to prevent the generation of new strong positive waves, allowing the reflected negative waves to fully exert their cancelation effect on the pressure buildup. This "active peak-shifting" mechanism is the core reason why the maximum pressure is mitigated. Finally, in the last 31.3% of the time, the nozzle rapidly closes the remaining 40% of the stroke. By this time, the kinetic energy of the water column has largely dissipated, and negative reflected waves dominate the transient flow field. The fast closing in this final phase compensates for the time lost during the middle phase and quickly cuts off the residual jet without triggering secondary pressure peaks.

5. Conclusions

This study focused on the water-hammer risk induced by normal shutdown of large-capacity, high-head Pelton turbines with long and complex water-conveyance systems, where rapid closure is required but excessive transient pressure must be avoided. A coupled simulation–optimization framework was established by integrating a one-dimensional elastic water-hammer model solved via the MOC with a Pelton turbine boundary model and further embedding the solver into the multi-objective optimizer NSGA-II to search for non-linear nozzle-closing laws. The main conclusions are summarized as follows:

(1) Under the baseline linear nozzle-closing strategy, the total closing time was 18.15 s, and the maximum head in front of the needle reached 744.17 m, indicating a pronounced pressure rise during shutdown. For the same total closing time, typical two-stage strategies ("fast–slow" and "slow–fast") produced higher pressure peaks than the linear law, implying that coarse redistribution may aggravate constructive wave superposition in long-penstock systems. In contrast, the three-stage "fast–slow–fast" law reduced the maximum head to 733.93 m (a reduction of 10.24 m compared with the linear case), whereas the "slow–fast–slow" strategy resulted in an unfavorable peak of 752.64 m. It shows that effective pressure suppression relies on a finer stage design that can modulate wave interaction, rather than a linear strategy.

(2) By coupling NSGA-II with the MOC-based approach and parameterizing the closing trajectory into 10 equal-stroke segments, a Pareto set was obtained that explicitly quantifies the trade-off between total closing time and maximum transient head. Compared to the baseline linear strategy, the optimized trajectory reduced the total closing time by 7.22% and mitigated the net water-hammer pressure rise by 13.40%. The optimization autonomously converged to a refined "fast-slow-fast" non-linear pattern. Physical analysis reveals that the intermediate "slow" phase plays a critical role in active peak-shifting. It effectively staggers the generation of new pressure waves from the return of upstream-reflected waves, thereby preventing severe constructive superposition while allowing the final fast phase to recover shutdown efficiency.

Overall, the proposed framework provides a practical approach for designing non-linear nozzle-closing laws for high-head Pelton units, offering simultaneous benefits in shutdown rapidity and water-hammer mitigation for long-penstock hydropower systems.

Although the 1D MOC framework is well-established, the absence of field validation data for this specific plant remains a limitation, which will be addressed in future work once the station is commissioned.

Author Contributions: Conceptualization, J.S. and C.L.; methodology, J.S. and C.L.; software, J.S. and C.L.; validation, J.S., C.L. and L.C.; formal analysis, J.S. and C.L.; investigation, J.S., C.L. and L.C.; resources, L.C.; data curation, J.S., C.L. and L.C.; writing—original draft preparation, J.S.; writing—review and editing, C.L.; visualization, J.S. and C.L.; supervision, C.L. and L.C.; project administration, L.C.; funding acquisition, L.C. All authors have read and agreed to the published version of the manuscript.

Funding: This research was funded by China Datang Corporation, grant number DTXZ-2021-10054.

Data Availability Statement: The original contributions presented in the study are included in the article; further inquiries can be directed to the corresponding author.

Conflicts of Interest: Author Lei Chen was employed by the company China Datang Corporation Science &Technology General Research Institute Hydropower Branch. The remaining authors declare that the research was conducted in the absence of any commercial or financial relationships that could be construed as a potential conflict of interest. The authors declare that this study received funding from China Datang Corporation. The funder was not involved in the study design, collection, analysis, interpretation of data, the writing of this article or the decision to submit it for publication.

References

1. Amir, M.; Deshmukh, R.G.; Khalid, H.M.; Said, Z.; Raza, A.; Muyeen, S.M.; Nizami, A.-S.; Elavarasan, R.M.; Saidur, R.; Sopian, K. Energy storage technologies: An integrated survey of developments, global economical/environmental effects, optimal scheduling model, and sustainable adaption policies. *J. Energy Storage* **2023**, *72*, 108694. [CrossRef]
2. Wu, B.; Shi, J.; Yang, J.; Zhang, H.; Liu, Z.; Tan, L. A Deep Reinforcement Learning Approach for Real-time Optimization Scheduling of Large Capacity Pelton Turbines. *J. Phys. Conf. Ser.* **2025**, *3150*, 012027. [CrossRef]
3. Lupa, S.-I.; Gagnon, M.; Muntean, S.; Abdul-Nour, G. The Impact of Water Hammer on Hydraulic Power Units. *Energies* **2022**, *15*, 1526. [CrossRef]
4. Pal, S.; Hanmaiahgari, P.R.; Karney, B.W. An Overview of the Numerical Approaches to Water Hammer Modelling: The Ongoing Quest for Practical and Accurate Numerical Approaches. *Water* **2021**, *13*, 1597. [CrossRef]
5. Wang, C.; Yang, J.-D. Water Hammer Simulation Using Explicit–Implicit Coupling Methods. *J. Hydraul. Eng.* **2015**, *141*, 04014086. [CrossRef]
6. Nicolet, C.; Greiveldinger, B.; Hérou, J.J.; Kawkabani, B.; Allenbach, P.; Simond, J.-J.; Avellan, F. High-Order Modeling of Hydraulic Power Plant in Islanded Power Network. *IEEE Trans. Power Syst.* **2007**, *22*, 1870–1880. [CrossRef]
7. Adamkowski, A.; Henclik, S.; Janicki, W.; Lewandowski, M. Experimental Verification of 1D-Simulation of Water Hammer. *Appl. Sci.* **2024**, *14*, 7173. [CrossRef]
8. Vakil, A.; Firoozabadi, B. Investigation of valve-closing law on the maximum head rise of a hydropower plant. *Sci. Iran.* **2009**, *16*, 222–228.
9. Liu, L.; Fan, H.; Chen, N. Optimization of distributor closure law in pumped-storage stations. *J. Tsinghua Univ.* **2006**, *46*, 1892–1895.
10. Yu, X.; Zhang, J.; Miao, D. Innovative Closure Law for Pump-Turbines and Field Test Verification. *J. Hydraul. Eng.* **2015**, *141*, 05014010. [CrossRef]
11. Michele, S.; Sammarco, P. Weakly nonlinear theory of water hammer induced by slow valve manoeuvres. *J. Fluid Mech.* **2025**, *1021*, A36. [CrossRef]
12. Xin, Q.; Du, J.; Liu, M.; Liu, Y.; Huang, J.; Yu, W.; Yuan, F.; Wang, D.; Yang, X. Experimental study on the effects of two-stage valve closure on the maximum water hammer pressure in micro-hydroelectric system. *J. Water Process Eng.* **2024**, *65*, 105886. [CrossRef]
13. Zhang, L.; Li, M.; Tong, J.; Zhang, H.; Wang, Y.; Hao, B. Calculation and prevention of water hammer for long distance gravity flow water conveyance pipelines. *J. Water Resour. Water Eng.* **2023**, *34*, 121–126. (In Chinese)
14. Lai, X.; Li, C.; Zhou, J.; Zhang, N. Multi-objective optimization of the closure law of guide vanes for pumped storage units. *Renew. Energy* **2019**, *139*, 302–312. [CrossRef]
15. Shu, S.H.; Fan, H.; Zhang, B.; Wu, J. Application of genetic algorithm to the optimization of the closing of gates in pumped-storage power stations. *J. Tsinghua Univ.* **2000**, *40*, 35–38. [CrossRef]

16. Zhao, W.; Wang, L.; Zhai, Z.; Wang, Z. Application of Multi-Objective Optimized Methods in the Closure Law of Guide-Vanes. In *Proceedings of the Chinese Control and Decision Conference*; IEEE: New York, NY, USA, 2010; pp. 3552–3556.
17. Yi, B.; Liu, X.; Wang, X.; Zhang, L. Study on joint optimal operation of pumps and valves under phased shutdown of pumps based on the coati optimization algorithm. *J. Tsinghua Univ. (Sci. Technol.)* **2025**, *65*, 1868–1879. (In Chinese)
18. Zhou, J.; Xu, Y.; Zheng, Y.; Zhang, Y. Optimization of Guide Vane Closing Schemes of Pumped Storage Hydro Unit Using an Enhanced Multi-Objective Gravitational Search Algorithm. *Energies* **2017**, *10*, 911. [CrossRef]
19. Ye, J.; Zeng, W.; Zhao, Z.; Yang, J.; Yang, J. Optimization of Pump Turbine Closing Operation to Minimize Water Hammer and Pulsating Pressures During Load Rejection. *Energies* **2020**, *13*, 1000. [CrossRef]
20. Liu, Z.D.; Wan, H.; Tang, Y.D.; Li, G.J.; Wang, Y.C.; Luo, X.B.; Tan, L. Research on Multi-objective Optimal Control of Multi-nozzle Pelton Turbine Unit. *J. Phys. Conf. Ser.* **2025**, *3150*, 012055. [CrossRef]
21. Chaudhry, M.H. *Applied Hydraulic Transients*, 3rd ed.; Springer: New York, NY, USA, 2014.
22. Zhang, Z. *Pelton Turbines*; Springer: Cham, Switzerland, 2016.
23. Lohrasbi, A.; Attarnejad, R. Water Hammer Analysis by Characteristic Method. *Am. J. Eng. Appl. Sci.* **2008**, *1*, 287. [CrossRef]
24. Bujak, P.; Krause, S. Modelling Water Hammer Effects in Rising Pipeline Systems Using the PKP Method and the MOC. *Energies* **2025**, *18*, 5005. [CrossRef]
25. Zhang, X.; Cheng, Y.; Xia, L.; Yang, J.; Qian, Z. Looping dynamic characteristics of a pump-turbine in the S-shaped region during runaway. *J. Fluids Eng.* **2016**, *138*, 091102. [CrossRef]
26. Ciren, S.; Suo, Z.; Yu, J.; Cai, W. Research on governor transformation and control of multi-nozzle Pelton turbine units. *Small Hydropower* **2016**, *1*, 39–42. (In Chinese)
27. Deb, K.; Pratap, A.; Agarwal, S.; Meyarivan, T. A fast and elitist multiobjective genetic algorithm: NSGA-II. *IEEE Trans. Evol. Comput.* **2002**, *6*, 182–197. [CrossRef]

Disclaimer/Publisher's Note: The statements, opinions and data contained in all publications are solely those of the individual author(s) and contributor(s) and not of MDPI and/or the editor(s). MDPI and/or the editor(s) disclaim responsibility for any injury to people or property resulting from any ideas, methods, instructions or products referred to in the content.